Erzincan Üniversitesi
Fen Bilimleri Enstitüsü Dergisi
2024, 17(2), 563-572
ISSN: 1307-9085, e-ISSN: 2149-4584
Araştırma Makalesi

Erzincan University
Journal of Science and Technology
2024, 17(2), 563-572
DOI: 10.18185/erzifbed.1517346
Research Article

Synthesis of Tungsten Disulfide on B-N-Doped Carbon Nanotubes to Enhance the Electrochemical Performance of Supercapacitors

Yasar Ozkan YESİLBAG[1*], Fatma Nur TUZLUCA YESİLBAG[1], Ahmad HUSEYİN[2] and Ahmed Jalal Salih SALIH[2]

[1]Department of Physics, Erzincan Binali Yıldırım University, Erzincan 24100, Turkey
[2]Erzincan Binali Yıldırım University Graduate School of Natural and Applied Sciences, Department of Pyhsics, Erzincan 24100, Turkey

Received: 16/07/2024, **Revised:** 04/08/2024, **Accepted:** 23/08/2024, **Published:** 31/08/2024

Abstract

In this research, boron and nitrogen-doped carbon nanotubes (B-N-CNTs) were synthesized at 900°C using the FCCVD method. Carbon, nitrogen, and boron as source materials were simultaneously introduced using a batch-mode droplet reactor and ferrocene as a catalyst. B-N-CNTs were obtained with diameters ranging from 10 - 50 nm and lengths around 30 – 80 µm. These B-N-CNTs were thoroughly characterized and structurally analyzed. Subsequently, tungsten disulfide (WS_2) nanosheets on B-N-CNTs were synthesized using the hydrothermal method to design a composite material and were investigated as electrodes for supercapacitors. The morphological properties of B-N-CNT@WS_2 were determined by various analytical techniques such as XRD, FESEM, XPS, and EDS. B-N-CNT@WS_2 was investigated as an electrode for supercapacitors in two- and three-electrode cells. In the three-electrode cell, B-N-CNT@WS_2 exhibited a specific capacitance of 320 F g^{-1} at a current density of 0.5 A g^{-1}, while the two-electrode cell showed a capacitance of 41 F g^{-1}. The symmetric supercapacitor at a current density of 5 A g^{-1} exhibited excellent structural stability by preserving 90% of its specific capacitance after 9000 cycles in the 1 V potential range.

Keywords: B-N-CNTs, WS_2, composite electrode, supercapacitor

Süperkapasitörlerin Elektrokimyasal Performansının İyileştirilmesi için B-N-Katkılı Karbon Nanotüpler üzerine Tungsten Disülfürün Sentezi

Öz

Bu araştırmada, FCCVD yöntemi kullanılarak 900°C'de bor ve nitrojen katkılı karbon nanotüpler (B-N-CNT) sentezlenmiştir. Kaynak malzeme olarak karbon, nitrojen ve bor, katalizör olarak ferrosenin olduğu toplu modlu damlacık reaktörü kullanılarak eş zamanlı olarak dahil edilmiştir. Çapları 10 - 50 nm arasında değişen ve uzunlukları 30 - 80 µm civarında olan B-N-CNT'ler elde edilmiştir. Bu B-N-CNT'ler kapsamlı bir şekilde karakterizasyonu yapılmıştır. Daha sonra, B-N-CNT'ler üzerine tungsten disülfür (WS_2) nanotabakaları, kompozit bir malzeme tasarlamak için hidrotermal yöntem kullanılarak sentezlenmiş ve süperkapasitörler için elektrotlar olarak araştırılmıştır. B-N-CNT@WS_2'nin morfolojik özellikleri XRD, FESEM, XPS ve EDS gibi çeşitli analitik tekniklerle belirlenmiştir. B-N-CNT@WS_2, hem iki hem de üç elektrotlu hücrelerde süperkapasitörler için bir elektrot olarak araştırılmıştır. Üç elektrotlu hücrede, B-N-CNT@WS_2, 0.5 A g^{-1} akım yoğunluğunda 320 F g^{-1}'lik spesifik bir kapasitans sergilerken, iki elektrotlu hücrede 41 F g^{-1}'lik bir kapasitans göstermiştir. Simetrik süperkapasitör ise 5 A g^{-1} akım yoğunluğunda 1 V potansiyel aralığında 9000 döngüden sonra kapasitesinin %90'ini koruyarak mükemmel yapısal kararlılık sergilemiştir.

Anahtar Kelimeler: B-N-CNTs, WS_2, kompozit elektrot, süperkapasitör

*Corresponding Author: oyesilbag@erzincan.edu.tr
Yasar Ozkan YESİLBAG, https://orcid.org/0000-0002-2519-3078
Fatma Nur TUZLUCA YEŞİLBAĞ, https://orcid.org/0000-0003-4383-2432
Ahmad HUSEYİN, https://orcid.org/0000-0002-2260-2593
Ahmad Jalel Salih SALİH, https://orcid.org/0000-0002-1760-5423

1. Introduction

Due to the increasing demand for efficient and sustainable energy storage technology, driven by the escalating consumption of fossil fuels and their depletion, there is a growing search for alternative solutions and the development of new and environmentally energy sources (Wang et al., 2015; Tu et al., 2016). Alternative electrical energy emerges as the most popular option to address this issue as it is generated from clean and renewable sources such as wind and solar (Dai et al., 2016). Extensive efforts are being made to store electrical energy safely and environmentally, with batteries and supercapacitors being one solution (Choudhary et al., 2016). Supercapacitors, also known as double-layer capacitors, consist of opposing electrodes separated by an insulator (Tomko et al., 2011; Wu et al., 2012). Energy is stored in supercapacitors in the form of electric charges on the surface of the electrodes, allowing for rapid discharge when needed (Yesilbag et al., 2022). Supercapacitors are characterized by fast charge and discharge rates, long-term cycle life, and the ability to withstand many charge-discharge cycles compared to conventional batteries. However, they still suffer from lower energy storage capacity compared to batteries. Thus, efforts are focused on improving their performance for applications requiring large amounts of energy. Supercapacitors excel in their ability to store and release energy quickly and efficiently, making them ideal for various applications in renewable energy and energy storage systems (Tuzluca Yesilbag & Huseyin, 2024).

In recent years, researchers have focused on using nanomaterials as electrodes for supercapacitors (Kinoshita et al., 2019; Béguin et al., 2014). Nanomaterials emerge as an excellent option for manufacturing supercapacitor electrodes due to their excellent conductivity and large surface area (Li et al., 2018). Recently, hybrid nanomaterials with one-dimensional, two-dimensional, and three-dimensional structures have been synthesized to enhance the electrochemical performance of supercapacitors. Among the one-dimensional materials, carbon nanotubes (CNTs) and boron and nitrogen-doped carbon nanotubes (BCN) have shown promise as electrode materials for supercapacitors and batteries (Yesilbag et al., 2021). Also, WS_2 nanosheets were synthesized on reduced graphene oxide (RGO) using a molten salt process, exhibiting a high specific capacitance of 2508.07 F g^{-1} at a scan rate of 1 mV s^{-1} due to the synergistic effect of WS_2 and RGO (Kim et al., 2011; Zhang et al., 2014; Chen et al., 2011). CNTs were introduced to improve the conductivity of WS_2. WS_2@CNT exhibited good specific capacitance of up to 752.53 mF cm^{-2} at a scan rate of 20 mV s^{-1} (Yang et al., 2020).

In this study, boron- and nitrogen-doped carbon nanotubes were synthesized using the Floating Catalyst Chemical Vapor Deposition (FCCVD) system. The doping process enhances the nanotube electron and ion transport during charge and discharge, increasing mechanical flexibility and contributing to pseudocapacitance. Transition metal dichalcogenide (WS_2) was synthesized on B-N-CNT without additional treatment. B-N-CNT@WS_2 was examined as electrode materials for supercapacitors and exhibited good capacitive properties.

2. Materials and Methods

2.1. Synthesis of B-N Doping CNTs by Chemical Vapor Deposition:

B-N-CNTs were synthesized using the FCCVD method, which is a modified version of the chemical vapor deposition method. In batch-mode droplet reactor, methanol, boric acid, and acetonitrile were used as sources for B, N, and C, respectively. Ferrocene ($C_{10}H_{10}Fe$) was used as a catalyst. Initially, methanol (CH_3OH) and boric acid (H_3BO_3) were mixed in a weight ratio of 1%, and then acetonitrile (C_2H_3N) was added. 0.15 g of ferrocene powder was placed in a quartz tube at the front of the furnace. The mixed carrier gas (H_2=30 sccm, Ar=60 sccm) was initially sent upon reaching the desired temperature of 900°C. Then, the gas flow rate was changed to Ar=500 sccm and H_2=300 sccm, and ferrocene was vaporized to initiate the growth process of B-N-CNTs. The solution injection rate was 10 ml/hour. The growth process continued for half an hour, and then the process was stopped while the flow of gases continued Ar=60 sccm and H_2=30 sccm until it reached room temperature. B-N-CNTs were collected from the walls of the quartz tube.

2.2. Synthesis of Tungsten Disulfide (WS_2):

Tungsten disulfide nanosheets were synthesized using the hydrothermal method. In this method, 1 g of oxalic acid ($C_2H_2O_4$), 0.3 g of sodium tungstate dihydrate, and 0.4 g of thioacetamide were taken in 50 ml of deionized water and mixed for an hour at room temperature. Then, the solution was transferred to a Teflon-lined autoclave with a capacity of 100 ml and heated to 200 °C for 12 h. After the process, the powder was washed with water several times and dried in an oven at 60 °C for 24 h.

2.3. Electrochemical Measurements:

The electrode was coated on carbon cloth consisting of active material, carbon black, and binder (PDVF) with a weight ratio of 8:1:1. Sample areas of 1 × 1 cm^2 were immersed in the electrolyte and tested as working electrodes. Electrochemical measurements of cyclic voltammetry (CV) and galvanostatic charge-discharge (GCD) were performed using a three-electrode system with a platinum (Pt) counter electrode and Ag/AgCl reference electrode. A 6 M KOH solution was used as the electrolyte. Electrochemical impedance spectroscopy (EIS) was performed over a frequency range from 10 kHz to 10 mHz. The specific capacitance (C_s) was calculated from GCD curves using the following equations:

$$C=I\times t/m\times V$$

where I is the constant discharge current, t is the discharge time, V is the potential window, and m is the mass of the active material. Additionally, measurements were carried out in a symmetrically design two-electrode cell in a 6 M KOH electrolyte using B-N-CNT@WS_2 electrodes.

3. Results and Discussion

Figure 1 depicts the synthesis steps for the B-N-CNT@WS_2 electrode. Briefly, B-N-CNTs were synthesized via the FCCVD process, followed by powder collection, HCl washing, and sonication. After then, B-N-CNTs and WS_2 precursor materials was put into the autoclave for a hydrothermal growth.

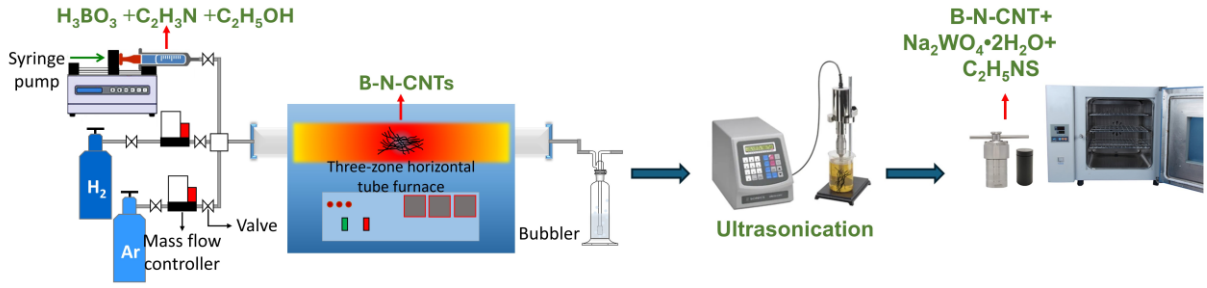

Figure 1. Schematic diagram of B-N-CNT@WS_2 synthesis.

In our previous study, B-N-CNTs were grown at 900°C and appeared as intertwined threads adhering to each other; hence, ultrasonic treatment was employed to separate them (Yesilbag et al., 2022). This process facilitates electron transfer on the one hand and provides a high surface area on the other hand. The FESEM images demonstrate the successful synthesis of B-N-CNT@WS_2, as shown in Figure 2 (a-c). The full area EDS analysis of B-N-CNT@WS_2 shown in Figure 3 showed that the atomic concentrations of W, S, B, C, N, and O were observed without any impurities.

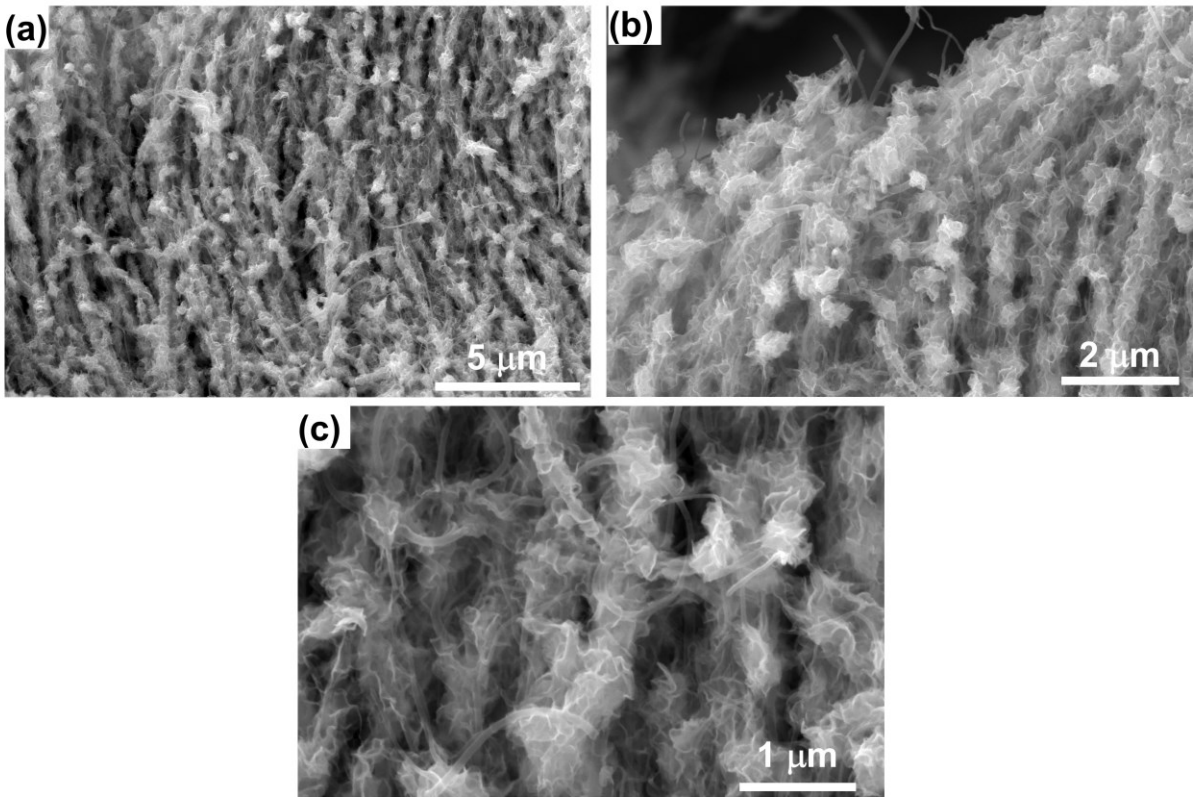

Figure 2. FESEM images for B-N-CNT@WS_2.

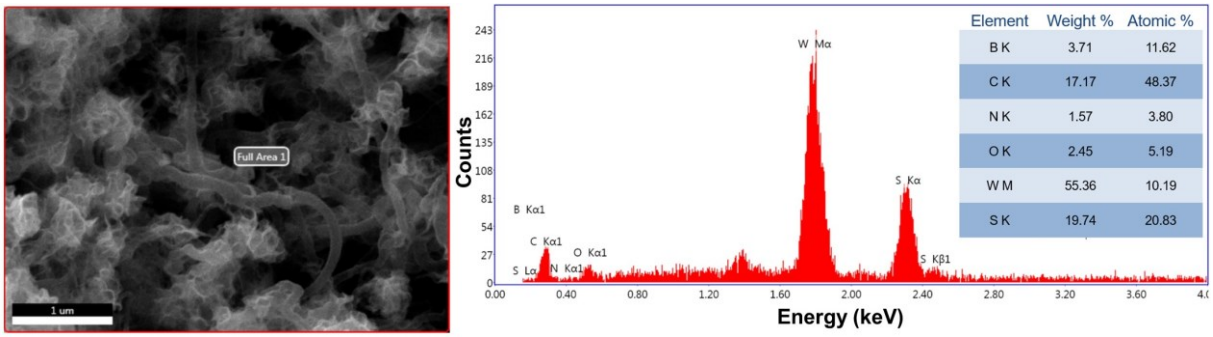

Figure 3. Full area EDS analysis for B-N-CNT@WS_2.

XRD analysis was conducted to analyze further and confirm B-N doping into the CNTs. Figure 4 shows an XRD pattern attributed to JCPDS card no: 41-1487 of graphitic structure B-N-doped carbon and JCPDS Card No: 84-1398 of WS_2, confirming the successful synthesis of B-N-CNT@WS_2.

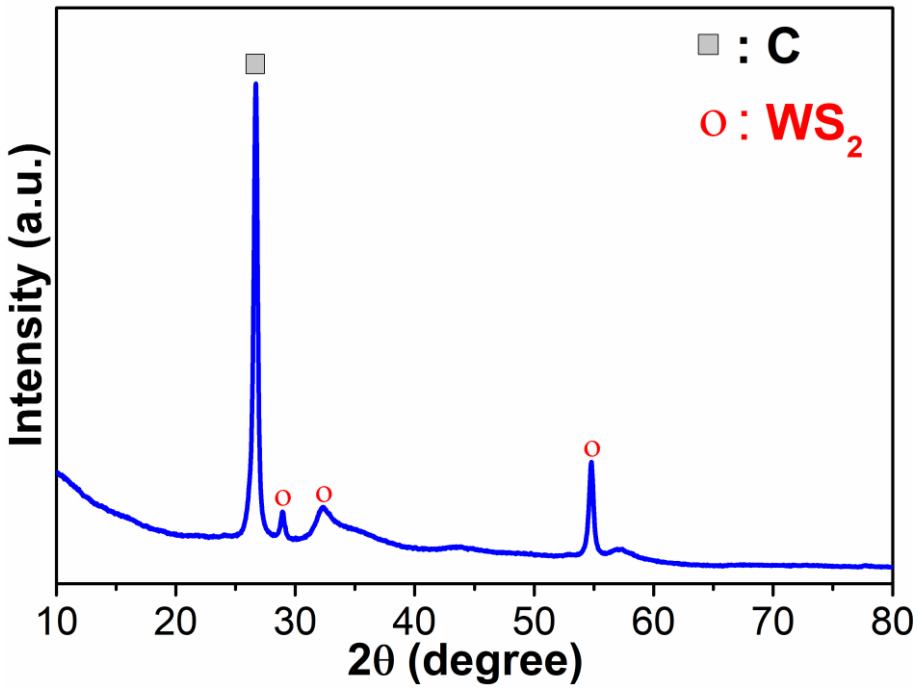

Figure 4. XRD analysis for B-N-CNT@WS_2 composite electrode material.

Through XPS analysis of B-N-CNT@WS_2, all elements B, C, N, W, S, and O appeared in the full spectrum, indicating the presence of peaks corresponding to B 1s, C 1s, N 1s, W 4f, S 2p, and O 1s (Figure 5 (a)). In the high-resolution XPS spectrum, the binding energies of C 1s, B 1s, and N 1s found at 285 eV, 185.5 eV, and 402 eV was shown in Figure 5 (b), (c), and (d), respectively. This indicates that boron and nitrogen bond to carbon. Additionally, peaks for W appeared at 36.4 eV and 34.5 eV, corresponding to W $4f_{7/2}$ W $4f_{5/2,}$ respectively (Figure 5 (e)). Moreover, in Figure 5 (f), the peaks for S appeared at 168.1 eV and 161.9 eV, corresponding to S $2p_{3/2}$ and S $2p_{1/2,}$ respectively, confirming the successful synthesis of WS_2.

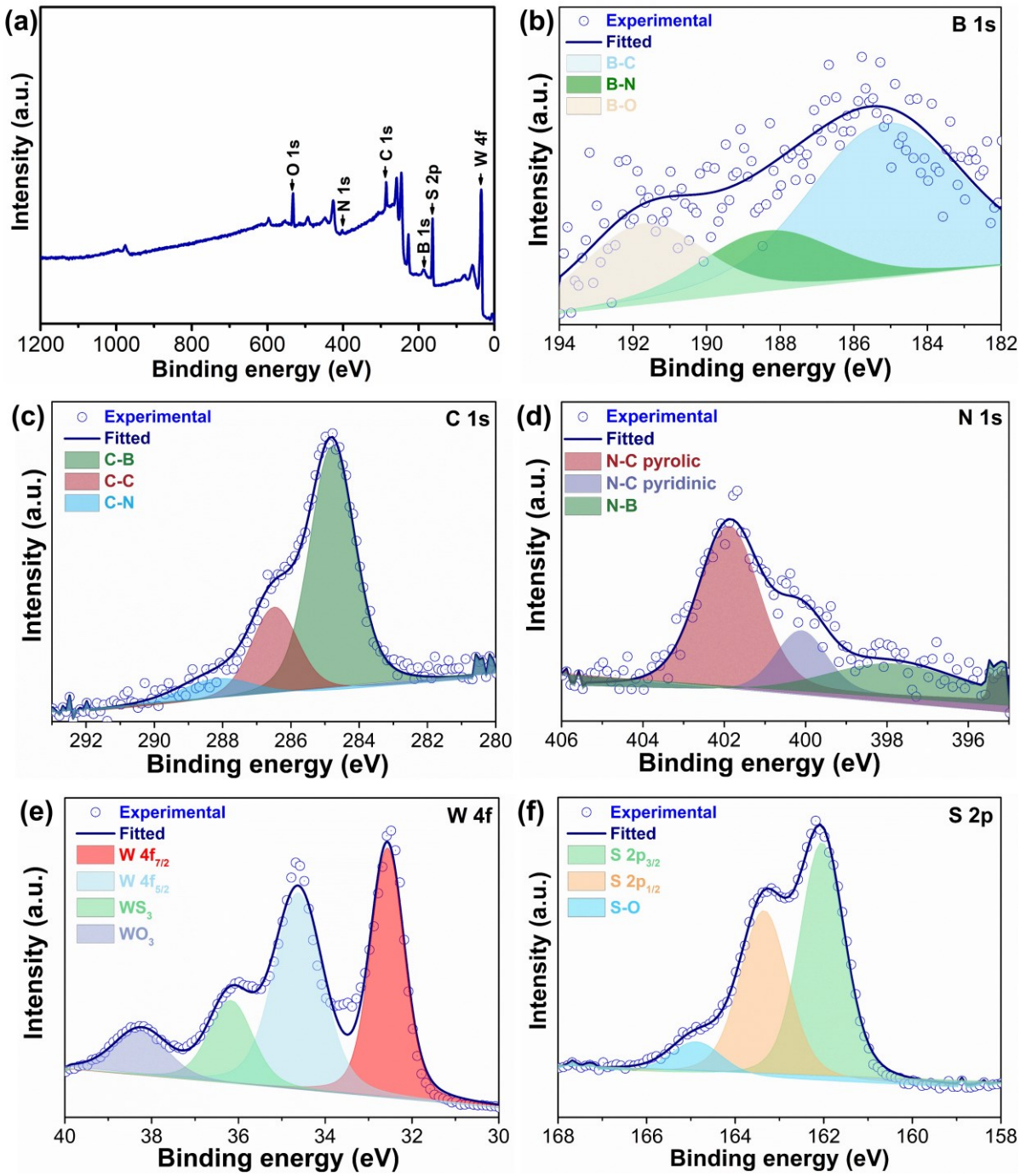

Figure 5. (a) XPS full spectrum of B-N-CNT@WS_2, the high-resolution spectrum of peaks (b) B 1s, (c) C 1s, (d) N 1s, (e) W 4f, and (f) S 2p.

Electrochemical measurements for the B-N-CNT@WS_2 electrode were conducted in a 6 M KOH electrolyte in a three-electrode system. In Figure 6 (a), the CV curves show broad shapes within the voltage range of -1.1 V to -0.2 V, indicating a mixture of EDLC and surface Faradaic processes occurring on the electrode surface. Small peaks are observed at -0.8 V and -0.5 V, corresponding to the surface oxidation and reduction processes of WS_2. Various scan rates 5-100 mV s^{-1} were applied, showing minimal changes in shapes, indicating capacitive properties and excellent performance. In Figure 6 (b), charge/discharge curves exhibit nearly symmetric triangular shapes, confirming the good capacitive behavior of the B-N-CNT@WS_2 electrode.

Figure 6 (c) illustrates the specific capacitance values at 0.5, 1, 2, 5, and 10 A g^{-1} current densities 320, 286, 210, 195, and 186 F g^{-1} respectively. Electrochemical behavior is further confirmed by EIS measurement shown in Figure 6 (d). The B-N-CNT@WS_2 electrode displays a parallel curve to the y-axis in the low-frequency range, indicating good capacitive behavior.

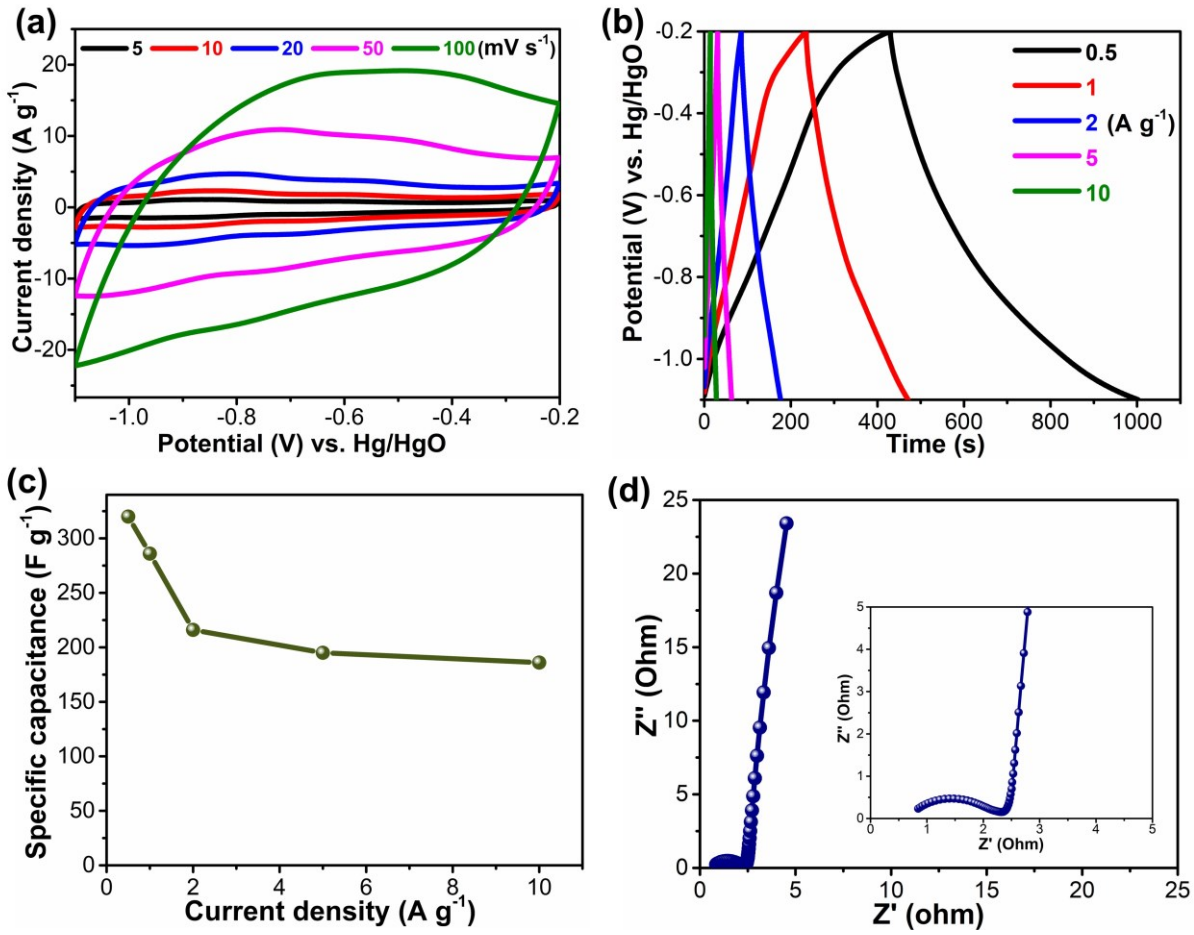

Figure 6. (a) CV curves at scan rates of 5-100 mVs^{-1}, (b) GCD curve at current densities of 0.5-10 A g^{-1}, (c) specific capacitance values, (e) Nyquist curves for EIS measurement (inset is enlarged high-frequency region).

A symmetrical supercapacitor (SSC) B-N-CNT@WS_2//B-N-CNT@WS_2 was assembled in two-electrode cell. CV and GCD measurements of the SSC were conducted within the voltage range 0-1 V, as shown in Figure 7 (a) and (b). The CV curves appeared rectangular, and the CV area increased with the scan rate, indicating capacitive behavior and reversibility. Figure 7 (c) shows the specific capacitance values of the SSC at current densities 0.5, 1, 2, and 5 A g^{-1} to be 41, 25, 20, and 18.4 F g^{-1}, respectively. Moreover, to evaluate the cycling stability of the SSC, a test was conducted at a current density of 5 A $g^{-1,}$ demonstrating a high stability of 90% after 9000 cycles, as shown in Figure 7 (d). In the EIS spectrum in Figure 7 (e), the intersection of the semicircle with the x-axis is ESR, and its value is 0.46 ohms, while the diameter of the semicircle is $R_{ct,}$ and its value is 0.51 ohms.

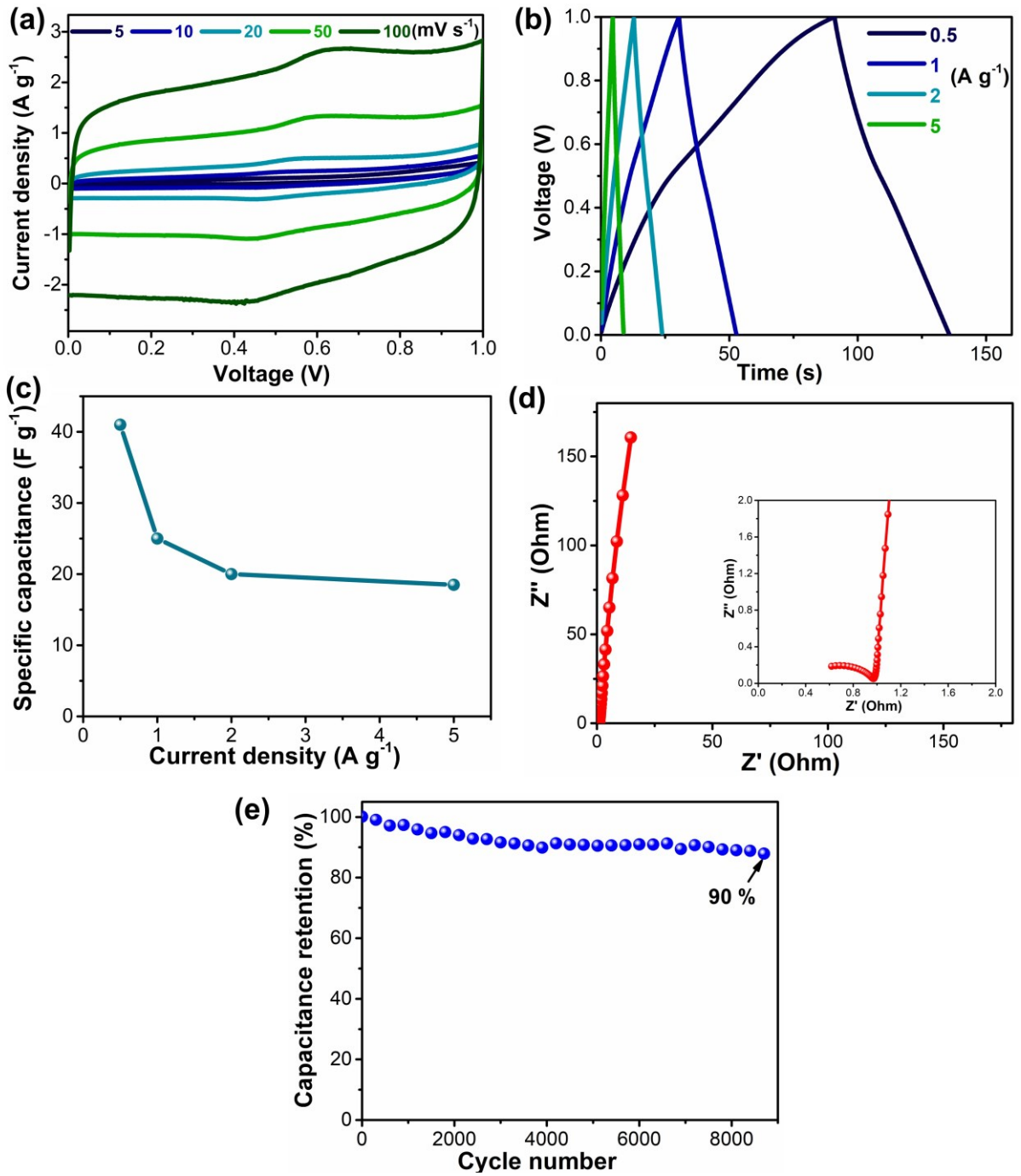

Figure 7. (a) CV curves at scan rates 5-100 mV s^{-1} for the SSC, (b) GCD curves at different current densities in the 0-1 V potential range, (c) specific capacitance values, (d) Nyquist plot, (e) Long-term cycling stability at 5 A g^{-1} current density.

4. Conclusion

In conclusion, the B-N-CNT@WS_2 electrode was synthesized in two stages. Initially, B-N-CNT was synthesized at a temperature of 900°C using the FCCVD method, followed by the WS_2 synthesis on the B-N-CNT surface via hydrothermal treatment. The B-N-CNT@WS_2 electrode was studied through structural and morphological analyses using characterization techniques such as XRD, FESEM, and XPS. WS_2 nanosheets were grown homogeneously on

BCN nanotubes, creating a synergistic effect. The B-N-CNT@WS_2 composite electrode shows a higher specific capacitance of 320 F g^{-1} at a current density of 0.5 A g^{-1}. Moreover, the SSC demonstrated the specific capacitance 41 F g^{-1} at a current density of 0.5 A g^{-1}, with a capacitance retention rate of 90% after 9000 cycles.

Acknowledgments

This work was supported by the Scientific and Technical Research Council of Turkey, TUBITAK, under Grant Number 217M323.

Ethics in Publishing

There are no ethical issues regarding the publication of this study.

Author Contributions

Yasar Ozkan Yesilbag: Ideas; formulation or evolution of overarching research goals and aims; Acquisition of the financial support for the project leading to this publication.

Fatma Nur Tuzluca Yesilbag: Preparation, creation, and presentation of the published work, specifically visualization/ data presentation.

Ahmad Huseyin: Performing the experiments and data collection.

Ahmed Jalal Salih SALIH: Performing the experiments and data collection.

5. References

Béguin, F., Presser, V., Balducci, A., & Frackowiak, E. (2014). Carbons and electrolytes for advanced supercapacitors. Advanced materials, 26(14), 2219-2251.

Chen, Z., Hou, L., Cao, Y., Tang, Y., & Li, Y. (2018). Gram-scale production of B, N co-doped graphene-like carbon for high performance supercapacitor electrodes. Applied Surface Science, 435, 937-944.

Choudhary, N., Li, C., Chung, H. S., Moore, J., Thomas, J., & Jung, Y. (2016). High-performance one-body core/shell nanowire supercapacitor enabled by conformal growth of capacitive 2D WS_2 layers. ACS nano, 10(12), 10726-10735.

Dai, Y., Wu, X., Sha, D., Chen, M., Zou, H., Ren, J., ... & Yan, X. (2016). Facile self-assembly of Fe_3O_4 nanoparticles@WS_2 nanosheets: a promising candidate for supercapacitor electrode. Electronic Materials Letters, 12, 789-794.

Kim, Y. S., Kumar, K., Fisher, F. T., & Yang, E. H. (2011). Out-of-plane growth of CNTs on graphene 2- for supercapacitor applications. Nanotechnology, 23(1), 015301.

Kinoshita, T., Karita, M., Nakano, T., & Inoue, Y. 2019. "Two step floating catalyst chemical vapor deposition including in situ fabrication of catalyst nanoparticles and carbon nanotube forest growth with low impurity level". *Carbon*, 144, 152-160.

Li, S., Zhang, N., Zhou, H., Li, J., Gao, N., Huang, Z., ... & Kuang, Y. (2018). An all-in-one material with excellent electrical double-layer capacitance and pseudocapacitance performances for supercapacitor. *Applied Surface Science*, *453*, 63-72.

Tomko, T., Rajagopalan, R., Aksoy, P., & Foley, H. C. (2011). Synthesis of boron/nitrogen substituted carbons for aqueous asymmetric capacitors. Electrochimica acta, 56(15), 5369-5375.

Tu, C. C., Lin, L. Y., Xiao, B. C., & Chen, Y. S. (2016). Highly efficient supercapacitor electrode with two-dimensional tungsten disulfide and reduced graphene oxide hybrid nanosheets. Journal of Power Sources, 320, 78-85.

Tuzluca Yesilbag, F. N., & Huseyin, A. (2024). Designing CuO@$MnCo_2O_4$ nanowire arrays electrode on copper foam and foil substrates via chemical synthesis methods for asymmetric supercapacitor. *Journal of Energy Storage*, *80*, 110148.

Wang, J., Li, X., Zi, Y., Wang, S., Li, Z., Zheng, L., ... & Wang, Z. L. (2015). A flexible fiber-based supercapacitor–triboelectric-nanogenerator power system for wearable electronics. Advanced Materials, 27(33), 4830-4836.

Wu, Z. S., Zhou, G., Yin, L. C., Ren, W., Li, F., & Cheng, H. M. (2012). Graphene/metal oxide composite electrode materials for energy storage. Nano Energy, 1(1), 107-131.

Yang, X., Li, J., Hou, C., Zhang, Q., Li, Y., & Wang, H. (2020). Skeleton-structure WS_2@CNT thin-film hybrid electrodes for high-performance quasi-solid-state flexible supercapacitors. *Frontiers in chemistry*, *8*, 442.

Yesilbag, Y. O., Yesilbag, F. N. T., Huseyin, A., & Ertugrul, M. (2022). The hierarchical synthesis of tungsten disulfide coated vertically aligned boron carbon nitride nanotubes composite electrodes for supercapacitors. *Journal of Energy Storage*, *52*, 104964.

Yesilbag, Y. O., Yesilbag, F. N. T., Huseyin, A., Salih, A. J. S., & Ertugrul, M. (2022). MnO_2 nanosheets synthesized on nitrogen-doped vertically aligned carbon nanotubes as a supercapacitor electrode material. *Journal of Alloys and Compounds*, *925*, 166570.

Zhang, X., Zhang, H., Li, C., Wang, K., Sun, X., & Ma, Y. (2014). Recent advances in porous graphene materials for supercapacitor applications. Rsc Advances, 4(86), 45862-45884.